

# Measurements of 14.1 MeV Neutron Reflection and Transmission for Carbon, Polyethylene, and Steel

Brandon Grogan<sup>a</sup>, Seth McConchie<sup>a,\*</sup>, John Mihalcz<sup>a</sup>, James Mullens<sup>a</sup>

<sup>a</sup> *Oak Ridge National Laboratory, Oak Ridge, TN, United States*

---

## Abstract

Fast and slow neutron return have been important in contributing to the effect of room return on unreflected subcritical and critical experiments. In addition, neutron reflectors are used with fissile material. As a first step in understanding fast neutron reflection, measurements were performed with time-tagged and directionally tagged 14.1 MeV neutrons from a D-T generator impinging on three common reflector materials. The time (energy) distribution of reflected fast neutrons was measured with respect to the emission of neutrons from the generator as a function of angle. The directional tagging assists in the removal of room return from these reflection measurements. In addition, the transmission was measured. This paper describes the experiment performed to characterize the neutron return from the common materials of carbon, polyethylene, and steel. The neutron return data presented in this paper can be used to benchmark calculational methods.

---

## 1. Introduction

Fast and slow neutron return have been important in contributing to the effect of room return on unreflected subcritical and critical experiments (Altschuler and Schuske, 1973; Bierman and Clayton, 1981; Bentley et al., 1994; Finfrock et al., 1997). In addition, neutron reflectors are used with fissile material (Mihalcz, 1972; Mihalcz, 1995; Waddell and Baltimore, 2001; Williams, 2003; Loaiza and Stratton, 2004). This paper describes an experiment that measured the transmission and reflection of 14.1 MeV neutrons emitted from a D-T neutron generator through carbon, polyethylene, and steel samples. These data can be used to benchmark calculational methods.

## 2. Experimental Setup

The experimental setup is shown in Fig. 1. Time- and direction-tagged neutrons produced by a D-T neutron generator (Thermo-Fisher API-120) with a pixelated alpha detector (YAP:Ce) and 5 mm target spot were incident upon a rectangular sample of each material measuring 45.7×45.7×7.6 cm-thick. The sample was placed at a 45° angle to the generator's long axis, and the sample face was 32 cm from the generator's target plane. The center of the sample was placed accordingly to account for the observed offset angle of 4.3° for the neutron cone. A multianode photomultiplier tube (Hamamatsu H8500) was used to divide the light from the alpha detector into eight horizontal pixels with a total width of 49 mm and a height of 6 mm.

---

\* Corresponding author, mcconchiesm@ornl.gov Tel: +1 (865) 576 9376; Fax: +1 (865) 576 8380.

The neutron cone covers a horizontal angle slightly more than  $45^\circ$  of the neutron cone and a vertical angle of approximately  $10^\circ$ .

An array of  $2.5 \times 2.5 \times 15.2$  cm-thick plastic scintillators (Scionix Holland V25.4B150-1EP-XNEG) was placed behind the sample to measure the neutron transmission. Each of the 18 detectors in the array was on an arc 85 cm from the target spot. A  $25.0 \times 25.0 \times 8.2$  cm-thick liquid scintillator (Scionix Holland V250 A32/3M-LS-XNEG) was placed diagonally to the generator to measure the neutron reflection. The face of the sample was 102 cm from the face of the liquid scintillator. A 10.4-cm tungsten cube was used to shield the liquid scintillator from the generator line-of-sight (does not look like it does in Fig.1). The middle of the generator and detectors were 110 cm from the floor.

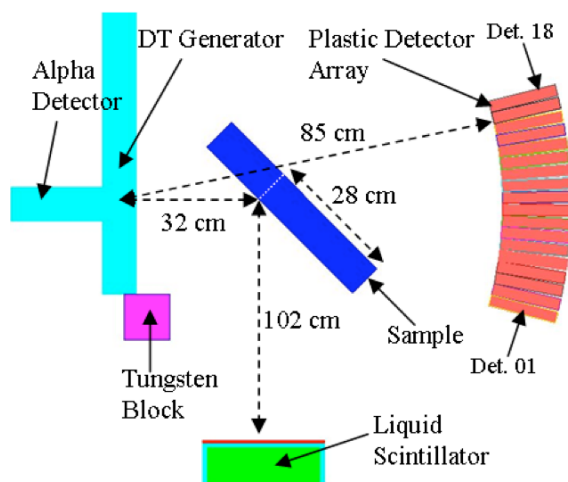


Fig. 1. Experimental setup of the reflection and transmission measurements for carbon, polyethylene, and steel samples. The detectors are identified by their order in the array. This image is not shown to scale.

The signals from the alpha detector, plastic scintillators, and liquid scintillator were passed through constant fraction discriminators (Ortec CFD 935) and then input to the NMIS processor (Mihalcz et al., 2000). NMIS measured the time correlations between events in the alpha detector and events in each detector of the array and events in the liquid scintillator. The timing uncertainty in the measurements is approximately 1 ns. Measurements were also made with pulse shape discrimination to distinguish between the neutrons and gamma-rays from the liquid scintillator.

### 3. Transmission Measurements and Analysis

The energy thresholds of the 18 plastic scintillators were set using a  $^{252}\text{Cf}$  time-of-flight measurement. Fig. 2 shows the neutron efficiency as a function of energy for the detectors. For these measurements the energy threshold is approximately 500 keV. Fig. 2 also shows that the response is roughly matched for all detectors.

Two sets of measurements were made with the 18 detectors in order to obtain a full transmission view of each sample. The array was offset by  $\pm 5.0^\circ$  from the axis connecting the generator target spot and the center of the detector array in order to cover the  $45^\circ$  horizontal angle. Each detector was sampled with four sub-positions corresponding to  $\frac{1}{4}$  of a detector ( $\sim 0.5^\circ$ ). Therefore, measurements were made at  $\pm 4.3^\circ$ ,  $\pm 4.8^\circ$ ,  $\pm 5.3^\circ$ , and  $\pm 5.8^\circ$ . For each angle, the measurement times were 4.3 minutes for each sample and 1.7 minutes for no sample.

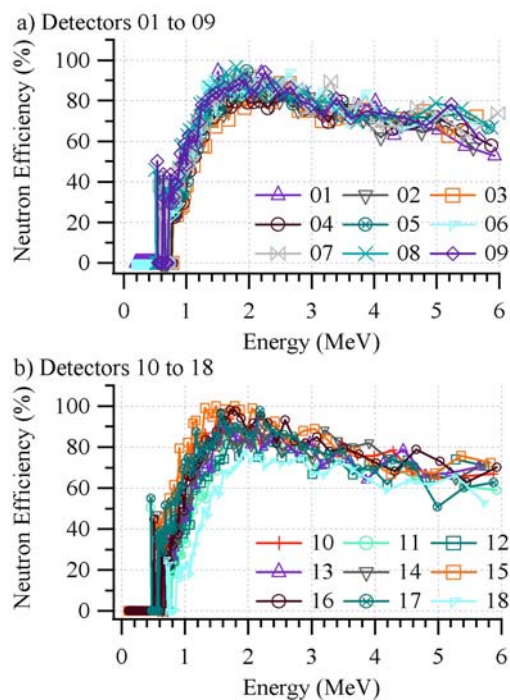


Fig. 2. Neutron energy efficiency for the 18 plastic scintillator detectors using  $^{252}\text{Cf}$  time-of-flight measurement. Because  $^{252}\text{Cf}$  fission neutrons are emitted isotropically, contributions include direct transmission and scattering of neutrons from the detectors and surroundings.

Because 14.1 MeV neutrons travel 5.1 cm/ns, a pulse in an array detector is expected at approximately 17 ns when correlated with an alpha event. An example of the correlation between the first array detector at  $-5.8^\circ$  and alpha pixel 1 is shown in Fig. 3. The attenuation is calculated as:

$$\text{Attenuation} = \Sigma_{tot} x = -\ln(I_{sample}/I_{void}) \quad (1)$$

where  $\Sigma_{tot}$  is the total macroscopic cross-section,  $I_{sample}$  is the number of transmitted counts when the sample is present, and  $I_{void}$  is the number of transmitted counts with no sample present. The total counts in each detector were calculated by integrating the peak from  $-4$  ns to  $+3$  ns around the time location corresponding to the maximum counts. The neutron attenuation for each sample is shown in Fig. 4. Pixels 2 through 8 give the transmission through sample. Pixel 1 does not view the sample and is not shown. Pixel 2 has reduced attenuation because it is viewing the edge of the sample.

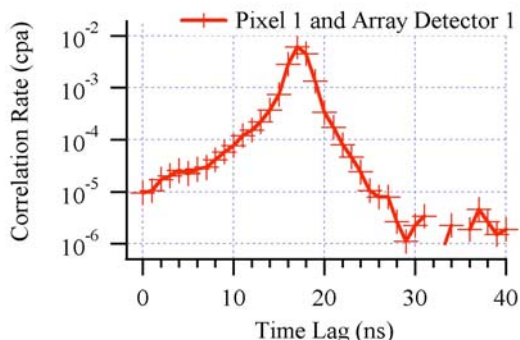


Fig. 3. Correlation counts per alpha event (cpa) between alpha pixel 1 and array detector 1 at  $-5.8^\circ$ . The neutron transmission peak appears at  $\sim 17$  ns. The accidental coincidence level has been removed.

The observed and expected attenuations for pixel 5, shown in Table 1, agree well. For all samples, the attenuations are lower than the expected attenuation. The discrepancies between measured and expected are a result of forward scattering of the 14.1 MeV neutrons in each sample. These neutrons arrive at approximately the same time as unscattered neutrons and reduce the measured attenuation. The largest discrepancy is for the steel sample, because elastic scattering is more forward peaked for iron than for carbon.

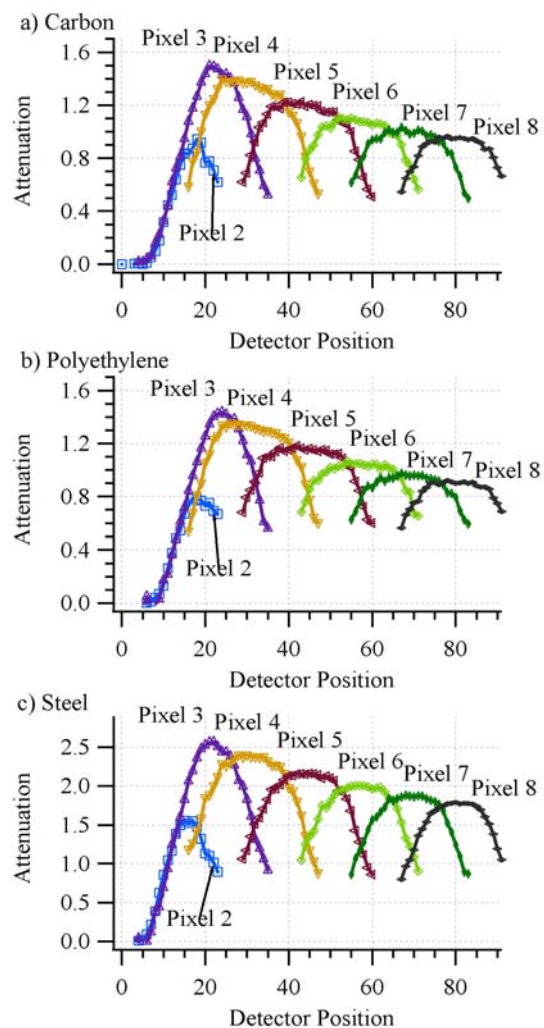


Fig. 4. Attenuation measured at each detector position for the samples. Pixel 1 does not view the sample, and pixel 2 has reduced attenuation because it is viewing the edge of the sample.

Table 1

Measured sample attenuation for pixel 5. The observed attenuations agree well with the expected attenuations, but are reduced due to the forward scattering of the 14.1 MeV neutrons. Total cross-sections were obtained from ENDF/B-VI.

Material	Density (g/cc)	Nuclei dens. (nuclei/b-cm)	$\sigma_{tot}(b)$ @ 14 MeV
Carbon	1.75	0.088	1.30
Polyethylene	0.94	0.121	

C		0.040	1.30
H		0.081	0.69
Steel	8.0	0.086	2.60
Material	$\Sigma_{tot}$ ( $\text{cm}^{-1}$ )	Attenuation ( $x = 10.7$ cm)	Measured Attenuation
Carbon	0.114	1.22	1.19
Polyethylene	0.108	1.16	1.15
C	0.052	0.56	
H	0.056	0.60	
Steel	0.224	2.40	2.15

#### 4. Reflection Measurements and Analysis

Time correlation data was collected for the liquid scintillator without pulse shape discrimination at the same time the transmission data was collected for each of the eight angles. The reflection data were added together for all eight angles to produce a composite data set representing 34.1 minutes of measurement time. Then the correlation data for all pixels were then added together to show the effect of pixelization. The data was recollected with pulse shape discrimination.

The radiation that appears in the time correlation data are elastically scattered neutrons, gamma-rays resulting from neutron inelastic scattering in the sample, and neutrons resulting from inelastic scattering and other reactions. Timing calibration was checked using these features in the data for pixels 2 and 8. The distance from the generator target spot to the sample in view of pixel 8 is 26 cm. Therefore, the time required for a 14.1 MeV neutron to travel to the sample is 5.1 ns. A gamma-ray resulting from neutron inelastic scattering in the sample travels 109 cm to the liquid scintillator for a travel time of 3.6 ns. An event occurs in the liquid scintillator approximately 8 to 9 ns after an alpha particle event.

The arrival time of an elastically scattered neutron is calculated by determining the final energy of the scattered neutron. In the center of mass frame, the final energy,  $E_f$ , is given by (Duderstadt and Hamilton, 1976):

$$E_f = (1/2)[(1+\alpha)+(1-\alpha)\cos\theta_{cm}]E_i \quad (2)$$

where  $E_i$  is the initial energy,  $cm$  is the scattered angle in the center of mass frame, and  $\alpha$  is given in terms of the target nucleus atomic weight,  $A$ , as  $((A-1)/(A+1))^2$ . For moderately large target nuclei, including carbon and iron,  $\theta_{cm} \sim \theta_{lab}$ , where  $\theta_{lab}$  is the scattering angle in the laboratory reference frame. In the experimental setup, neutron elastic scattering events in the liquid scintillator originating from the sample require that lab  $\theta_{lab} \sim \pi/2$ . For  $^{12}\text{C}$  and  $^{56}\text{Fe}$ , the final energies are 12.0 MeV and 13.5 MeV, respectively. Therefore, an event occurs in the liquid scintillator approximately 28 ns and 27 ns after an alpha event for the carbon and steel samples, respectively.

The event times for pixels 2 and 8 are shown in Table 2. The event time ranges for elastically scattered neutrons are 28 to 29 ns for  $^{12}\text{C}$  and 27 to 28 ns for  $^{56}\text{Fe}$ . The event time ranges for gamma-rays from neutron inelastic scattering are 8 to 14 ns. The event time distributions for the samples are shown in Fig. 5. A feature for pixel 2 appearing at  $\sim 20$  ns is due to gamma-rays resulting from neutron inelastic scattering in the detectors of the scintillator array. The composite event time distributions for all pixels are shown in Fig. 6.

Table 2

Pixel 2 and pixel 8 neutron and gamma event times in the liquid scintillator for each sample. The distance from the generator to portion of the sample in view of pixel 2 (pixel 8) is 54 cm (26 cm). The distance from the portion of the sample to the liquid scintillator is 85 cm (108 cm).

Material	$E_f$ (MeV)	n Event Time (ns)	$\gamma$ Event Time (ns)
Pixel 2			
Carbon	12.0	28.1	8.7
Polyethylene			
C	12.0	28.1	8.7
Steel	13.5	26.8	8.7
Pixel 8			
Carbon	12.0	28.5	13.4
Polyethylene			
C	12.0	28.5	13.4
Steel	13.5	27.5	13.4

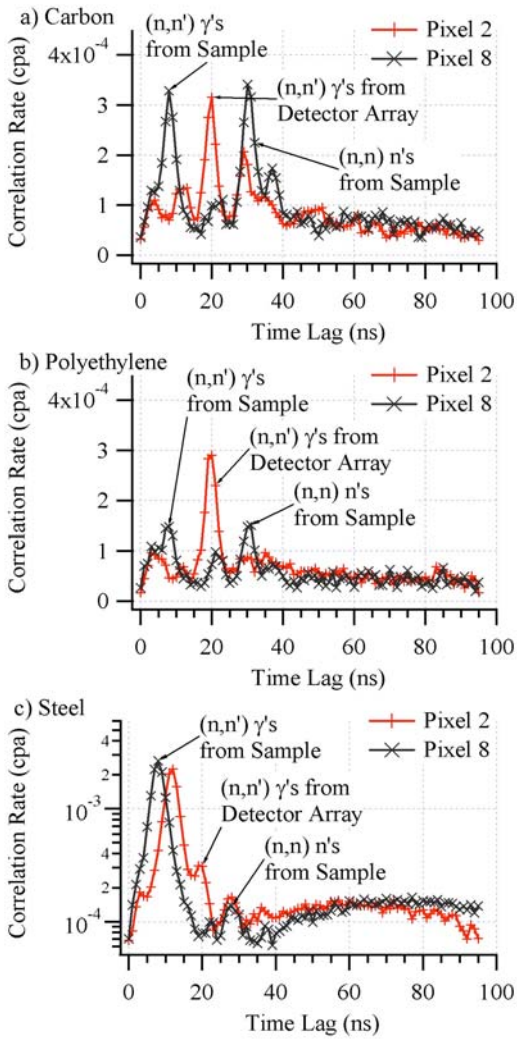


Fig. 5. Time distributions for pixel 2 and pixel 8 events correlated with events in the liquid scintillator.

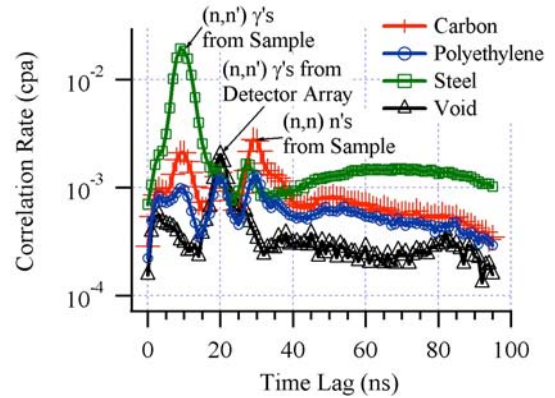


Fig. 6. Composite event time distributions for all alpha pixels. The gamma and neutron features are less distinguishable as compared to the pixelated distributions.

The settings for the pulse shape discrimination module (RIS Corp. 1568) were determined using a  $^{252}\text{Cf}$  source 1 meter away from the liquid scintillator. For these measurements, the PSD was set such that gamma events in the neutron channel were reduced to  $4 \times 10^{-3}$  compared to no PSD. The neutron efficiency as a function of energy for these setting is shown in Fig. 7. The neutron events in the gamma channel were reduced to  $6 \times 10^{-3}$  compared to no PSD. The relative gamma efficiency was near 100% for this neutron event reduction factor.

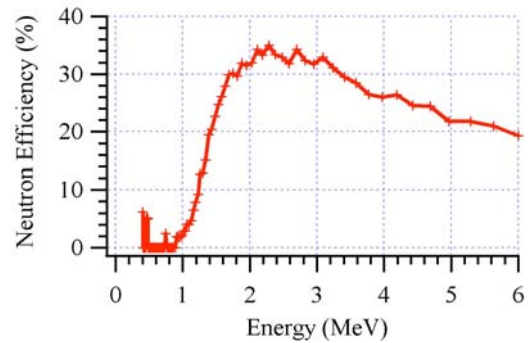


Fig. 7. Neutron efficiency of the liquid scintillator as a function of energy for the PSD setting such that gamma events in the neutron channel were reduced to  $4 \times 10^{-3}$  compared to no PSD.

The time distributions with pulse shape discrimination are shown in Fig. 8. The distributions show that carbon reflects the most number of fast neutrons, while iron reflects the most number of slower neutrons. Integrating the elastic scattering neutron peak  $\pm 2$  ns from the maximum

value gives  $6.3 \times 10^{-4}$  counts per alpha event (cpa) for carbon,  $2.6 \times 10^{-4}$  cpa for polyethylene, and  $2.8 \times 10^{-4}$  cpa for steel. Carbon enhances the elastically scattered neutron return by a factor of 2.4 over polyethylene and 2.2 over steel. In contrast, steel returns a larger number of neutrons from other reaction channels, such as (n,2n) and (n,n'), compared with carbon and polyethylene. Overall, steel enhances the total neutron return by a factor of 1.2 over carbon and 1.8 over polyethylene.

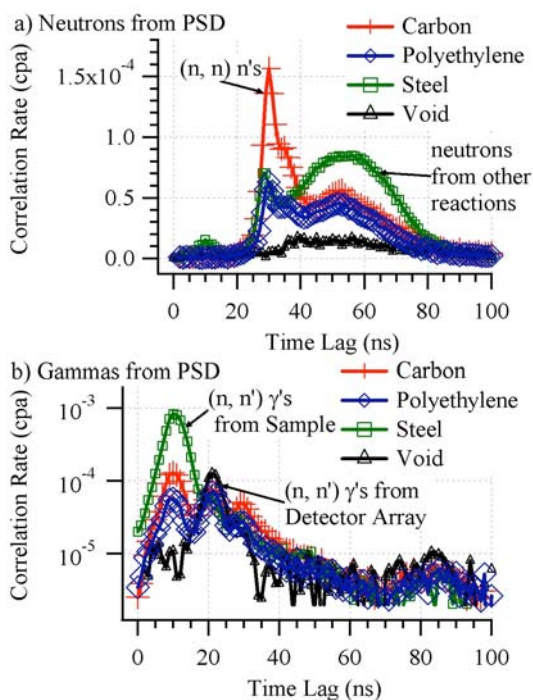


Fig. 8. Neutron and gamma time distributions using PSD with the liquid scintillator. Carbon enhances the elastically scattered neutron return by at least a factor of 2 compared to polyethylene and steel. However, steel returns a larger number of neutrons from other reaction channels.

## 5. Conclusion

This paper describes the measurement to characterize the reflection and transmission of carbon, polyethylene, and steel samples. The attenuation factor for each sample was calculated using the transmission data and agreed reasonably well with the expected values. The reflection data demonstrated that the carbon enhances the

elastically scattered neutron return by a factor of 2.4 over polyethylene and 2.2 over steel. In contrast, steel returns a larger number of neutrons from other reaction channels compared with carbon and polyethylene. Overall, steel enhances the total neutron return by a factor of 1.2 over carbon and 1.8 over polyethylene.

## Acknowledgement

This work was supported by National Nuclear Security Administration office of Facility and Infrastructure Acquisition and Operation (NA-17) and the NNSA Y-12 Site Office.

## References

- Altschuler, S.J., Schuske, C.L., 1973. A study of criticality parameters affecting the handling and storage of fissile metal. *Nucl. Technol.* 18, 55-62.
- Bentley, C. et al., 1994. Shutdown mechanisms for a hypothetical criticality accident involving HEU powder: preliminary results. *Trans. Am. Nucl. Soc.* 70, 188-189.
- Bierman, S.R., Clayton, E.D., 1981. Criticality experiments with subcritical clusters of 2.35 and 4.31 wt%  $^{235}\text{U}$ -enriched  $\text{UO}_2$  rods in water with steel reflecting walls. *Nucl. Technol.* 54, 131-144.
- Duderstadt, J.J., Hamilton, L.J., 1976. *Nuclear Reactor Analysis*, Wiley, New York.
- Finrock, S. et al., 1997. Impact of drum storage on criticality accident alarm systems. *Trans. Am. Nucl. Soc.* 77, 251-252.
- Loaiza, D.J., Stratton, W., 2004. Criticality data for spherical  $^{235}\text{U}$ ,  $^{239}\text{Pu}$ , and  $^{237}\text{Np}$  systems reflector-moderated by low capturing-moderator materials. *Nucl. Technol.* 146, 143-154.
- Mihalcz, J.T., 1972. Criticality of graphite- and polyethylene-reflected uranium (93.2%)-metal cylinders and annuli. *Nucl. Sci. Eng.* 49, 489-504.
- Mihalcz, J.T., 1995. A small graphite-reflected  $\text{UO}_2$  assembly. *Proceedings of The Fifth International Conference on Nuclear Criticality Safety* 1, 6/11-17.
- Mihalcz, J.T., et al., 2000. Physical description of nuclear materials identification system

- (NMIS) signatures. Nucl. Instr. Meth. A 450, 513-555.
- Rose, P.F. (Comp. and Ed.), 1991. Neutron-induced reaction file: ENDF-201, ENDF/B-VI Summary Documentation, BNL-NCS-17541, 4<sup>th</sup> ed.
- Waddell, M.W. Jr., Baltimore, W.D., 2001. Effects of concrete reflector composition in nuclear criticality safety calculations of LEU systems. Trans. Am. Nucl. Soc. 85, 165-166.
- Williams, M.M.R., 2002. The effect of random geometry on the criticality of a multiplying system V: influence of the reflector. Nucl. Sci. Eng. 143, 1-18.